

for publication in the  
Journal of Geophysical Research

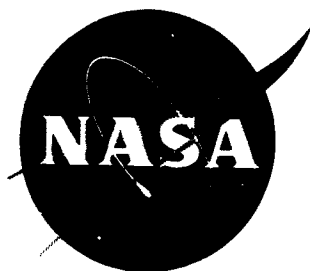
N65-89074

~~X64-12055~~ \*

Code 2A

(NASA TM X-54,006)

NASA TM X-54,006



SATELLITE OBSERVATIONS OF THE GEOMAGNETIC  
FIELD DURING MAGNETIC STORMS

8195109 E. J. Smith  
(Space Technology Laboratories, Inc.)  
Redondo Beach, California

(JPL)  
C. P. Sonett and J. W. Dungey (Imperial coll.)  
Space Sciences Division / Ames Research Center  
National Aeronautics and Space Administration

December 1963

Presented -- not p

Submitted for  
Publication

Available to NASA Offices and  
NASA Centers Only

NATIONAL AERONAUTICS AND SPACE ADMINISTRATION

SATELLITE OBSERVATIONS OF THE GEOMAGNETIC  
FIELD DURING MAGNETIC STORMS<sup>†</sup>

E. J. Smith<sup>1</sup>  
Space Technology Laboratories, Inc.  
Redondo Beach, California

C. P. Sonett and J. W. Dungey<sup>2</sup>  
Space Sciences Division, Ames Research Center  
National Aeronautics and Space Administration  
Moffett Field, California

ABSTRACT

12055  
Explorer 6 satellite data and surface magnetograms are used to study the gradual and sudden commencement geomagnetic storms of August 16-18, 1959. Analysis of these data provides the following conclusions:

1. The geomagnetic field was strongly perturbed but retained its essentially dipolar character out to geocentric distances of 8 earth radii.
2. A long period variation in the distant field coincided with  $D_{st}$  at the surface. The magnitude of the main-phase decrease at  $\sim 4R_E$  was  $\sim 2.5$  times larger than at the surface. Variations in the field direction at  $\sim 7R_E$  correlate with half-day variations in (a) the horizontal component at the surface and (b) the 3 hour K index.
3. Large irregular field fluctuations with periods exceeding one minute were characteristic of the storm period.

*Author*

---

<sup>†</sup>Portions of this paper were presented at the International Conference on Cosmic Rays and the Earth Storm, Kyoto, Sept. 1961 [Smith and Sonett, 1962].

<sup>1</sup>Permanent address: Space Sciences Div., Jet Propulsion Laboratory, Pasadena, California.

<sup>2</sup>Permanent address: Dept. of Physics, Imperial College, London.

~~Available to NASA Offices and  
NASA Centers Only.~~

4. The large-scale storm field was qualitatively similar to the disturbance field observed previously on nonstorm days. The disturbance field appeared to evolve from quiet to disturbed conditions followed by a gradual recovery.

## INTRODUCTION

Simultaneous measurements of the field at the surface and in the magnetosphere are essential to a better understanding of magnetic storms, since the solar effects responsible for storms can be strongly modified by a complicated interaction with the earth's outer atmosphere. Space probes, Pioneer 1 and Lunik 2 [Sonett, Judge, Sims, and Kelso, 1960; Krassovsky, 1960], traversed the distant geomagnetic field during nonstorm intervals. Pioneer 5 and Lunik 1 were launched during the recovery phases of a storm [Coleman, Sonett, Judge, and Smith, 1960] and Vanguard 3 (apogee ~10,000 km) measured the field above the ionosphere during an interval which included several moderate magnetic storms [Heppner, Stolarik, Shapiro, and Cain, 1960]. Explorer 6 made the first, repetitive measurements of the earth's field, between 4 and 8 earth radii, during a magnetic storm.

The satellite magnetic field data obtained by Explorer 6 at geocentric distances between 4 and  $8R_E$  (earth radii) during a severe magnetic storm are used below to study the gross characteristics of the large-scale storm field surrounding the earth. The physical origin of the storm field is investigated, including the possible existence of a main phase ring current. Long-period variations in the distant field are also compared with variations in the intensity of the outer radiation zone during the storm. Some of the data to be discussed were published previously in a preliminary report [Smith and Sonett, 1962].

## BACKGROUND

### Instrumentation

The detecting element of the magnetometer, a solenoid wound on a high permeability core, was attached to the shell of the spin-stabilized spacecraft which rotated 2.7 times per second. In an ambient stationary magnetic field, a sinusoidal voltage was generated with a frequency equal to the spin rate and an amplitude proportional to  $B_{\perp}$ , the component of the magnetic field perpendicular to the spacecraft spin axis (see fig. 1). The electronics consisted of an amplifier having a pass band centered at the spin frequency and a quasilogarithmic gain achieved by using an AGC loop. This extended the dynamic range of the magnetometer to 3 orders of magnitude so that fields could be measured over an extended range of altitudes.

The magnetometer coil constant, the numerical relation between field strength and the induced voltage, was determined by comparing the voltages generated when the search coil and a standard air-core coil were simultaneously rotated in the earth's field in a region where gradients were small. Sinusoidal input voltages were used to obtain steady-state electronic calibration. (The transient response of the magnetometer is not pertinent to this paper and will be discussed elsewhere.) In a given field, the output signal depended on the spin rate of the spacecraft and was only slightly dependent on the temperature of the electronics which was checked by means of several temperature sensors located inside the spacecraft. The satellite spin rate was the number of cycles of the telemetered sinusoid in a given time period. Further details of the equipment and its calibration are reported elsewhere [Judge, Sims, and McLeod, 1960].

Early recognition of the importance of directional data [Sonett, Judge, and Kelso, 1959] led to the inclusion of a photodiode sun scanner and phase comparator.

This instrument provided a phase reference, based on the solar direction, and determined, in flight, the directional variations in  $B_1$ . The merit of including this type of instrument has been supported by subsequent events, and now sun scanners are standard for spinning spacecraft magnetic field orientation.

The phase comparator measured the angle,  $\phi$ , between  $B_1$  and  $S_1$ , where  $S_1$  is the projection into the spacecraft equatorial plane of a unit vector pointing in the direction of the sun (see fig. 1). Hereafter,  $\phi$  is called the phase angle. It is the magnetic declination in spacecraft coordinates referred to the spacecraft-sun direction, and it depends on the orientation of the spacecraft spin axis.

The phase comparator input signals were the search coil sinusoid and a sequence of pulses generated by a photodiode when illuminated by solar radiation once per spacecraft revolution (fig. 2). The photodiode pulse and a pulse coincident with the zero-voltage crossing of the search coil sinusoid operated Schmidt triggers that controlled the state of a flip-flop. The output, obtained by integration of the flip-flop output signal, was a d-c voltage proportional to the time delay between the two pulses. Except for very small fields, the phase comparator output was independent of the magnitude of the search coil sinusoid and the measurement of  $\phi$  was independent of  $B_1$ .

The search coil and phase comparator analog voltages, which were frequency modulated and transmitted continuously, were received at one or more STL ground stations (England, Florida, Hawaii, and Singapore) for approximately 18 hours of each day. The search coil sinusoid was also converted to a slowly varying d-c voltage by a peak detector and filter and was digitized inside the spacecraft along with the phase comparator output. The transmissions of binary-coded digital data, which were commanded from the ground at irregular intervals, were used primarily to check the quality and accuracy of the telemetered analog data.

### Orbital Parameters

After Explorer 6 was launched in August 1959, much time and effort was expended in refining the ephemeris because of perigee drag fluctuations and solar-lunar perturbations, a poorly understood subject in 1959. With the establishment of an accurate orbit and a precise spin axis orientation, the more subtle effects in the data, such as the properties of the disturbance field near the geomagnetic equator, were made accessible.

The Explorer 6 orbit (apogee, 48,000 km; perigee, 6740 km) was highly eccentric. The orbital plane was inclined  $47^\circ$  to the geographic equator and apogee was at geographic latitude  $-20^\circ$ . The spacecraft crossed the equatorial plane at geocentric altitudes of 7200 and 30,000 km. Figure 3 shows the projection of the orbit onto the surface of the earth.

The satellite was launched from Atlantic Missile Range at 1345 GMT on August 7, 1959. Since perigee occurred at about 0900 hours local time, apogee was located on the opposite side of the earth at 2100 hours local time. On August 7, the projection onto the geographic equatorial plane of the semimajor axis of the orbit made an angle of  $\sim 135^\circ$  with respect to the earth-sun direction. This angle decreased by approximately  $1^\circ$  per day. The right ascension and declination of the spin axis were  $217^\circ$  and  $23^\circ$ , respectively.

The orbital period,  $12\text{-}3\frac{1}{4}$  hours, had an important effect on the instantaneous location of the spacecraft in geomagnetic coordinates. Because the earth's magnetic pole is inclined  $11\text{-}1\frac{1}{2}^\circ$  with respect to the rotation axis, the geomagnetic latitude of a given orbital position underwent a semidiurnal variation as large as  $23^\circ$ . However, as the period was nearly 12 hours, the rotation of the geomagnetic field and the orbital position of the spacecraft after two complete revolutions were only slightly asynchronous. This prompted us to divide the data

obtained on odd-numbered and even-numbered passes into two separate groups in order to isolate temporal changes in the geomagnetic field more clearly.

#### MAGNETIC CONDITIONS AT THE EARTH'S SURFACE

August 12, 13, and 14 were among the five quietest days in August [Lincoln, 1960] (fig. 4). On August 15, a gradual commencement storm was reported at some stations. At approximately 0400 on August 16, a sudden commencement storm began and continued until the end of the 17th or beginning of the 18th. This storm was classed as severe (corresponding to a K-index of 8 or 9). Huancayo reported a moderate, gradual commencement storm which began at 0635 on August 18 and ended at 2000 hours the same day. A moderately severe, sudden commencement storm began on August 20 at 0412. There is no general agreement as to when this storm ended. (Some stations estimated that it ended on the 20 while others recorded disturbed conditions until August 24.) August 27 and 28 were the two quietest days of the month. A moderately severe ( $K = 6, 7$ ), sudden commencement storm began on September 3 at 2159 and continued until September 5 or 6. The discussion which follows is concerned primarily with the severe magnetic storm of August 16.

#### Review of the Explorer 6 Data Obtained on Nonstorm Days

In the preliminary analysis of the data the magnitude,  $B_1$ , and direction,  $\phi$ , of the observed field were compared with the magnitude and direction of the extrapolated geomagnetic field [Sonett, Smith, Judge, and Coleman, 1960; Sonett, Smith, and Sims, 1960; Smith, Coleman, Judge, and Sonett, 1960]. An 8 coefficient, spherical-harmonic expansion of the surface field [Vestine, 1959] was used to derive a version of the geomagnetic surface field extrapolated to the satellite

position and resolved into the spacecraft coordinate system for comparison with the measured field. This field is labelled  $G_1$  and has spacecraft declination,  $\varphi_G$ .

Discrepancies between  $B_1$ , the measured component, and  $G_1$ , the extrapolated one, were observed throughout most of the trajectory. Below  $5R_E$ ,  $B_1$  tends to exhibit the same altitude dependence as  $G_1$  but to have a somewhat larger magnitude. Beyond approximately  $5R_E$ , there was a marked disparity between  $B_1$ ,  $G_1$ , and their spacecraft declinations,  $\varphi$  and  $\varphi_G$ .

An important consequence of the AGC loop is that the relative and absolute accuracy of measurement increased with increasing altitude. For example, a change of 1 percent in the output voltage corresponded to  $300\gamma$  in a  $5000\gamma$  field (approximate altitude, 12,000 km), and to only  $3\gamma$  in a  $100\gamma$  field (approximate altitude, 38,000 km). The differences between  $B_1$  and  $G_1$  beyond  $5R_E$  corresponded to large fractional changes (15 to 20 percent) in the magnetometer output signal. The experimental results suggested that the extraterrestrial field was essentially dipolar out to  $5R_E$ , deviating progressively at greater altitudes. (The deviation between  $G_1$  and  $B_1$  depends strongly on the direction of  $B_1$ , as well as on its magnitude.) A preliminary survey of data obtained throughout a 6-week interval showed that these differences were characteristic. Perturbations in  $B_1$  and  $\varphi$  were always noted, although their shapes varied from day to day and were strongly dependent on the geometry of the experiment.

A perturbation field based on an equatorial current with a finite, circular cross section and constant current density was used to explore possible causes of the observed differences. The field due to the current was computed at points on the trajectory and added vectorially to the geomagnetic field; a coordinate transformation was then performed to yield theoretical values of  $B_1$  and  $\varphi$ .



Reasonable agreement between the data and the model calculations was obtained for a westward current of  $5.10^6$  amperes centered at  $10R_E$  [Smith, Coleman, Judge, and Sonett, 1960].

Perturbations in the distant geomagnetic field were also subsequently observed by Pioneer 5 on the sunward side of the earth. When the same mathematical model was applied to the Pioneer 5 magnetometer data obtained inside the geomagnetic field, reasonable agreement was again obtained between the calculated and observed  $B_1$  for a westward current of  $5.10^6$  amperes centered at  $8R_E$  and extending from 5 to  $11R_E$ .

These model calculations, employing an ad hoc current, were justifiably criticized as ignoring an important feature of currents associated with trapped particles. The diamagnetic character of the trapped particles should lead to a maximum reduction of the geomagnetic field at the peak of the particle kinetic energy distribution. Akasofu and Chapman (1961) compared the Explorer 6, August 9 data with a computed field based on a model radiation zone. Their results place the particles at  $\sim 6R_E$  and suggest the total current was  $\sim 2.10^6$  amperes. Similarly, Apel, Singer, and Wentworth (1962) derived a distribution of trapped particles corresponding to the Pioneer 5 magnetometer data and found it to be centered at  $\sim 6R_E$ . Although both these calculations employed ideal rather than observed particle distributions and did not take account of geometrical effects associated with the data, such as the geomagnetic latitude and spin axis orientation of the spacecraft, they undoubtedly lead to a more realistic estimate of where the particles causing the Explorer 6 and Pioneer 5 field deformations were located than our preliminary model calculations. For example, compare the vector disturbance field computed by Akasofu, Cain, and Chapman (1961) (their fig. 1) with the Explorer 6 vector measurements [Smith, 1962, fig. 1].

It should be noted that the model calculations were applied to data obtained under disturbed magnetic conditions. The Pioneer 5 data were acquired during the recovery of a moderate magnetic storm. The Explorer 6 data obtained on August 9 were initially regarded as nonstorm data because a preliminary classification did not list August 9 as a disturbed day. However, as figure 4 shows, the  $K_p$  index reached a value of 4 during the period the data were obtained. All periods in which  $K_p$  exceeded 4 included storms.

#### THE EXPERIMENTAL DATA

The data in figure 5 were obtained on three successive days during the severe SC storm which began on August 16.

The storm data show the same qualitative features as the measurements made on nonstorm days (e.g., see fig. 1 in Sonett, Smith, Judge, and Coleman, 1960). The fine structure appearing in figure 5, for example, a variation of several hundred gamma that occurred at 30,000 km on August 17, may be the result of either spatial or temporal variations and is a subject of special interest investigated separately in connection with bay-like, polar storm variations [Smith and Judge, 1961].

In interpreting the data, it is assumed that the field was perpendicular to the equatorial plane on the geomagnetic equator for both quiet and storm time fields. Therefore, the scalar field measured at the equator completely specified the resultant field. For nonequatorial points of observation, variations in  $B_1$  were caused by a change in the direction as well as in magnitude of the field. Thus, treating the equatorial measurements separately will simplify the interpretation of the experimental data. The next section describes the time dependence of the field magnitude near the geomagnetic equatorial plane. This is followed

by a discussion of field direction at points of observation below the equatorial plane. The centered dipole approximation of the geomagnetic field is used to define the geomagnetic equator.

#### Variation in the Magnitude of the Near-Equatorial Field During the Storm

Figure 6(a) shows the time variation of the field magnitude in the outer radiation zone. Each datum was obtained from a measurement of  $B_1$  at a geocentric distance of approximately 24,000 km or  $4R_E$  (the actual radial distance varied between 22,000 and 26,000 km). The corresponding value of the extrapolated geomagnetic field was computed and subtracted from  $B_1$ . The differences ( $\Delta B_1 = B_1 - G_1$ ) are plotted in figure 6(a) for approximately the first two weeks of Explorer 6 observations. Since the observed field at 24,000 km tends to exceed the extrapolated surface field on magnetically quiet days, a feature of the data that could be caused by a lack of good absolute accuracy at this altitude, the data in figure 6(a) were adjusted so that  $\Delta B_1 = 0$  on the quietest days of the month (August 11-12) by subtracting the amount by which  $B_1$  exceeded  $G_1$  on August 11 from all the differences. The digital data appearing in figure 6(a), which were similarly adjusted, provide data at times for which no analog data were available.

Figure 6(b) is the time variation of the horizontal component of the surface field. Each datum, the daily mean value of the horizontal intensity at Huancayo, Peru, (geomagnetic latitude,  $\delta_M$ ,  $-0.6^\circ$ ) obtained by averaging the hourly mean values over each Greenwich day, has been plotted at 1200 GMT. This procedure produced a reasonable representation of long period changes in the earth's field. The variation in mean horizontal intensity has also been biased so that  $\Delta H = 0$  on August 11-12.

The outstanding feature of the Huancayo data is the superimposed magnetic storms of August 15-20. The storm period was preceded and followed by quiet intervals during which the horizontal component rose to its highest values (August 14-15, 26-28). The effect of the SC storm which began on August 16 is particularly noticeable.

Figure 6(c), which is a plot of the smoothed  $D_{st}$  curve derived by Chapman and Akasofu [Arnoldy, Hoffman, and Winckler, 1960], shows the history of the August 16 storm in greater detail. The data are averages of the horizontal component measured at 12 observatories well distributed in latitude and longitude.

The long-period variation of the storm field at the surface coincides with a similar variation at an altitude of  $\sim 4$  earth radii (24,000 km). A comparison of figures 6(a), (b), and (c) indicates that  $B_1$  undergoes a main phase decrease and recovery at  $\sim 4R_E$  which is essentially coincident with  $D_{st}$  at the surface. The magnitude of the main phase decrease is  $\sim 140\gamma$  at the surface and  $\sim 360\gamma$  at  $4R_E$ , that is, approximately two and one-half times as large.

#### Variation in the Direction of the Extraterrestrial Field During the Storm

Figure 7 shows the departure of the observed field direction from the direction of the extrapolated geomagnetic field and contrasts the departures on storm days and quiet days. The experimental measurements obtained from the magnetic field aspect indicator (or phase comparator) are shown as a function of altitude for three orbital passes. Also shown are theoretical values of the phase angle for the extrapolated geomagnetic field ( $\varphi_G$ ).

At geocentric distances of less than 10,000-15,000 km,  $\varphi = \varphi_G$  because of the "stiffness" of the geomagnetic field near the earth (i.e., a transverse disturbance field of several hundred gamma would not produce an observable change in the direction of the dipole field lines). Fortunately, the same range of angles ( $150^\circ < \varphi < 300^\circ$ ) was observed near the earth and at great distances. Thus, the agreement between  $\varphi$  and  $\varphi_G$  near perigee provides a check on the consistency of the aspect indicator calibration.

At large distances from the earth, where Explorer 6 was at southern geomagnetic latitudes, the phase deviation,  $\Delta\varphi = \varphi - \varphi_G$ , was negative. On the geomagnetic equator ( $\delta_M = 0$  is indicated in figs. 8 through 11 and the geomagnetic latitude of the spacecraft as it travelled from 20,000 km to apogee is shown in fig. 14),  $\Delta\varphi$  was either zero (passes 16, 18, and 20) or slightly negative (orbits 15, 17, 19, 21, and 22).

The extent by which  $\varphi$  differed from  $\varphi_G$  depended, in part, on the trajectory of the Explorer 6 (i.e., the magnetic latitude of the spacecraft at a given altitude). There was also a time variation apparent in figure 7. Magnetic storms occurred August 17 and September 4, while August 27 was one of the quietest days of the month ( $A_p$  indices are included in the figure).

On August 27 and 13  $\Delta\varphi$  was smallest when, as figure 6 indicates, the horizontal intensity at the earth's surface rose to its highest value. These observations are qualitatively consistent with a decreased westward current in the magnetosphere.

Another feature of figure 7 was the occurrence of fine structure during the magnetic storms. Several distinct transients (such as those seen at 30,000 km on August 17 and at 42,000 km on September 4) correlated with pulsating magnetic bays in the antarctic [Smith and Judge, 1961], and transient increases in the Explorer 6 scintillator count rate. According to Rosen and Farley [1961], the occurrence of rapid variations in the scintillator count rate was typical of magnetically disturbed periods.

Figures 8 through 11 contain the phase angle data for eight successive orbital passes during August 15-18.  $\sum K_p$  is the sum of the 3 hour, planetary K indices during the 12-hour period corresponding to each orbital pass of the Explorer 6. The altitude at which the spacecraft crossed the geomagnetic equatorial plane is denoted in each figure by  $\delta_M = 0$  and an arrow (see fig. 14 for the position of the spacecraft at other geomagnetic latitudes).  $\theta_M$  is an angle between  $\hat{\omega}$ , the Explorer 6 spin axis, and  $\hat{n}$ , the normal to the local magnetic meridian plane (fig. 12). The meridian plane contains the local field direction and the center of the earth. The perpendicular to the magnetic meridian plane is given by  $\hat{e}_B \times \hat{e}_R$ , where  $\hat{e}_B$  is a unit vector in the direction of the extrapolated geomagnetic field and  $\hat{e}_R$  is a unit radial vector from the earth's center to the spacecraft. The extent to which the spacecraft spin axis was rotated out of the magnetic meridian plane at different points along the trajectory is indicated by  $\theta_M$ . The angle,  $\lambda_S$ , is obtained when the earth-sun vector and the satellite radius vector are projected onto the equatorial plane (fig. 13).

As discussed earlier, the data are divided into two groups in order to minimize trajectory effects. Figures 8 and 9 contain only the odd-numbered passes which generally occurred during the first half of the Greenwich day, whereas figures 10 and 11 contain even-numbered passes. There were small progressive changes

in the geomagnetic coordinates of the spacecraft at a given point on the trajectory on the odd-numbered and even-numbered orbits taken alone. In figures 14 and 15 the altitude at which  $\delta_M$  was zero progressed to higher altitudes during the odd-numbered passes and to lower altitudes during the even-numbered passes.

Figures 8 through 11 show a progressive enhancement of  $\Delta\phi$  during the storm with a subsequent return to prestorm values. This may be seen if we consider a given  $\Delta\phi$  (e.g.,  $\Delta\phi = -20^\circ$ ), which moved toward lower altitudes during the main phase of the storm ( $\Sigma K_p$  increasing) and returned to higher altitudes during the recovery phase ( $\Sigma K_p$  decreasing).

Figure 16 provides an alternative view of the variations in  $\Delta\phi$  during the storm. Figure 16(a) is a plot of  $\Delta\phi$  at a given altitude (40,000 km) as a function of time. Figure 16(b) shows the simultaneous variation in the horizontal intensity at the earth's surface. The data are hourly mean values of  $H$  at Huancayo. The diurnal variation has been removed. Figure 16(c) is a plot of the corresponding values of the 3-hour index,  $K_p$ . The direction of the distant field was correlated with both variations in the horizontal component and the degree of agitation of the surface field.

This correlation appears to include the initial phase of the August 16 storm. However, the increase in  $\Delta H$  and decrease in  $\Delta\phi$ , observed during the first quarter of August 16, actually represented a superposition of two effects, the initial phase of the sudden commencement storm of August 16 and the recovery phase of the gradual commencement storm of August 15. The effect of the GC storm on the distant field can be seen in the first two data in figure 10 (August 15) and by comparing figures 8(a) and 10(a) (successive passes). An

inspection of ground station magnetograms shows that the GC storm was of short duration. Because the two storms overlap, it was not possible to isolate and study the effects of the initial phase of the SC storm. The subsequent data show the effect of the main phase decrease and recovery associated with the August 16 storm.

Simultaneous Variations in Field Magnitude and Peak  
Intensity of the Outer Radiation Zone

Figure 17(a) is the same as figure 6(d), that is,  $\Delta B_1$  at  $\sim 4R_E$ . Measurements of the peak intensity of the radiation particle fluxes in the outer zone are also shown. Figures 17(b), (c), and (d) are the Explorer 6 data obtained by the University of Minnesota Geiger tube, the University of Chicago proportional counter, and the Space Technology Laboratories scintillation counter. Prior to the storm of August 16, the primary peak in the outer zone was located at approximately 24,000 km, on the basis of Geiger tube data, [Arnoldy, Hoffman, and Winckler, 1960]. Thus, equatorial field measurements and Geiger tube measurements of the peak intensity occur in the same region of space and are essentially simultaneous. The peak of the outer zone as detected by the other two instruments was displaced slightly from 24,000 km [Fan, Meyer, and Simpson, 1960; Rosen and Farley, 1961].

During the storm main phase, there was a substantial decrease in the count rates of the University of Minnesota and University of Chicago experiments, followed by a large increase in the particle fluxes during the recovery phase of the storm. This behavior apparently is characteristic of the outer zone during a magnetic storm and has been observed by similar instruments on other satellites. The scintillator data departed from this general tendency during the main phase.



Figure 17 shows that the slow variations in particle intensity correlate with the variations in field magnitude at  $4R_E$ . The count rates of the Geiger tube and proportional counter decrease when the field magnitude decreases and the scintillator count rate increases slightly. When the field at  $4R_E$  recovers from the effect of the storm and returns to its prestorm value, all three particle count rates increase. However, the peak intensities in the outer zone are an order of magnitude larger than their prestorm values.

#### SUMMARY

The experimental data can be summarized as follows:

1. Long period time-dependent changes in the distant field coincided with  $D_{st}$  at the surface.
2. The magnitude of the main phase decrease in  $B_1$  was  $\sim 2.5$  times larger at  $\sim 4R_E$  than at the surface.
3. Irregular field fluctuations, with periods exceeding one minute, were observed during the storm. The largest fluctuations correlate with the occurrence of transient storm variations observed at the surface near the polar regions.
4. Variations in the direction of the field at  $\sim 7R_E$  correlate with half-day variations in (a) the horizontal component of the surface field, and (b) the three-hour, planetary K index.
5. The large scale perturbations of  $B_1$  and  $\phi$  during the storm were qualitatively similar to the perturbations observed previously on nonstorm days.

6. The  $D_{st}$  variations in the field magnitude at  $4R_E$  correlate with changes in the peak intensity of the outer radiation zone measured by three high-energy-particle detectors on Explorer 6. Two detectors show a decreased intensity during the storm when the field magnitude is depressed. All three detectors measured peak intensities which exceeded the prestorm values at the same time the field magnitude returned to its quiescent value.

## DISCUSSION

### Characteristics of the Large-Scale Storm Field

The storm data at 4 to  $8R_E$  and the world wide component of the surface storm field ( $D_{st}$ ) have the same time dependence. Furthermore, the variations at 1, 4, and 7 earth radii are essentially simultaneous, that is, possible time delays are much less than the characteristic period of the  $D_{st}$  variation. During the storm, the earth was immersed in a large-scale magnetic field that was manifest at the surface as the main phase decrease.

The characteristics of the  $D_{st}$  field at the earth's surface can be described simply. The field is approximately uniform and antiparallel to the earth's axis of rotation over the entire surface.

Ideally, a complete description is desired of the magnitude and direction of the  $D_{st}$  field in the space surrounding the earth. However, a complete description is not possible from a single orbiting satellite. It is particularly difficult to distinguish between a radial dependence and a dependence on latitude or longitude when the trajectory is a highly inclined ellipse such as the Explorer 6 orbit. In addition, in the instance of Explorer 6 useful data are restricted to portions of the orbit where the magnitude of the disturbance field was at least

several percent of the magnitude of the unperturbed geomagnetic field, as discussed previously. We can, however, infer several important properties of the large-scale storm field from the Explorer 6 data. Later magnetometer experiments can extend and improve this description.

We now show that near the equatorial plane at  $4R_E$ , the storm field ( $\Delta B$  as distinct from  $\Delta B_1$ ) was directed southward, was aligned with the local magnetic meridian plane, and had a magnitude of  $\sim 350\gamma$ . At 24,000 km,  $\theta_M$ , the angle between the spacecraft spin axis and the normal to the local magnetic meridian plane, was approximately  $105^\circ$ . Thus, the spin axis was nearly contained in the meridian plane. Consequently, field rotations out of, or transverse to, magnetic meridian planes were readily detectable. Conversely, along this part of the orbit, the phase angle was insensitive to rotations confined to magnetic meridian planes, which would leave  $\phi$  equal to  $\phi_G$ . The phase data (figs. 8 through 11) show that  $\Delta\phi$  did not exceed  $8^\circ$  during the storm. Therefore, any component of field rotation out of the magnetic meridian plane was small. The measurements give the disturbance nearly in the direction of  $G$  and show that it was small. It is unlikely that there is a strong disturbance parallel to the spin axis. The  $350\gamma$  decrease in  $B_1$  during the main phase implies a reduction in the magnitude of the field component parallel to  $G$  by a factor of approximately 2. Assuming that the field rotated without a change in magnitude implies a rotation of  $60^\circ$  which would produce a field with a large radial component near the equator. Such a field would differ greatly from the geomagnetic field. It would correspond, for example, to an interplanetary field or a strongly deformed magnetic tail existing at 24,000 km and lying in a magnetic meridian plane. The experimental evidence discussed above including the Explorer 6 trapped particle measurements,

makes it certain that the Explorer 6 was inside the geomagnetic field, particularly at 24,000 km. Therefore, it seems reasonable to conclude that the decrease in  $B_1$  is primarily a decrease in magnitude, that  $B$  and  $G$  were parallel near the equator, and that  $\Delta B(t)$  in figure 6 is approximately the magnitude of the time varying storm field near the geomagnetic equatorial plane. Small deviations in field direction cannot be ruled out but are not an essential feature of the arguments presented here.

### Ring Current

The disturbance observed during the storm is very suggestive of a ring current. To understand why the evidence is inconclusive, it is instructive to consider what observations would be needed for rigorous detection of this current. To deduce the current from measurements of the magnetic field, it is necessary to obtain  $\oint \mathbf{B} \cdot d\mathbf{S}$  round a closed curve, thus giving the current through that closed curve. Not only does Explorer 6 lack one component of  $\mathbf{B}$ , but no satellite moves in a closed curve suitable for this purpose. Such a measurement would, indeed, be awkward. One possibility might be to use two satellites, whose orbits are nearly coplanar and to compute the current through the lines between their orbits. In any event, quite accurate magnetic measurements would be needed. Here then we must be content to compare the observed field with that predicted for a ring current.

The ring current predicted is caused by trapped particles and can be regarded as arising either from their anisotropic pressure distorting the field hydromagnetically or as a combination of their drifts and diamagnetic effect. The latter is similar to pressure and causes an important depression of the field strength where the pressure is high, roughly according to pressure balance between particles

and field. Davis and Williamson [1963] have observed a population of trapped protons with a pressure substantially higher than that of the other known trapped particles. For  $L > 4$  their pressure is about one tenth of the magnetic pressure during quiet times and an increase in their pressure by a factor of 3 was observed during one storm. Akasofu [1963] has reviewed ring current theory and estimated the effect of the protons observed by Davis and Williamson. It is worth noting that whereas the disturbance at the ground corresponds to a westward current, the current due to trapped particles is eastward on the inner side of the particle distribution where the particle pressure is increasing with  $L$ . The westward current flows on the outer side and the resulting disturbance is illustrated by Akasofu's computations. He obtains for storm conditions in the equatorial plane a depression of  $100\gamma$  at the ground, a maximum depression of somewhat more than  $200\gamma$  between  $L = 3$  and  $4$  and a slight strengthening of the field beyond  $L = 6$ . The greater depression at  $L = 4$  than at the ground is in qualitative agreement with Explorer 6 and is due to the eastward current near in. The lack of detailed agreement could arise as follows. First, only protons of  $>100$  kev were observed by Davis and Williamson and softer protons might be important. Since the observed proton pressure went up to one third of the magnetic pressure, the pressure of softer particles could hardly be a dominant proportion, but it could change the maximum field depression from  $220\gamma$  to, say,  $350\gamma$ . Secondly, the storm observed by Explorer 12 was of course not the same as that observed by Explorer 6 and substantial differences between different storms seem to be allowable. Thirdly, Akasofu's calculation is not self-consistent. Finally, should the ring current be incapable of accounting fully for the observed disturbance on the trajectory of Explorer 6, the field farther out is known to be distorted in a quite different way. This distortion is not symmetric about the geomagnetic axis, but for the late

evening meridian of Explorer 6, there is some similarity with the changes of  $\phi$  observed near apogee, as this distortion will now be discussed briefly.

### Distortion of the Field in the Outer Magnetosphere

The solar wind, now certified by Mariner [Neugebauer and Snyder, 1962], distorts the magnetosphere. Many theoretical studies of this distortion have been published (e.g., Midgley and Davis, 1963) most of which have neglected any interplanetary magnetic field, though others have considered this (e.g., Dungey, 1963). Observations of this distortion were obtained from Explorers 10, 12, and 14. For comparison with Explorer 6, Explorers 10 and 14 are most relevant having apogee in the evening direction. Heppner, et al., [1963] found a boundary far out, but for the first 15 earth radii, the field strength was near the dipole value while the direction gradually swung round and pointed away from the earth (the apogees of Explorers 6, 10, and 14 were south of the equatorial plane). Cahill [1963] has published the results of two successive passes of Explorer 14 near the midnight meridian and separated by 36 hours. There was a magnetic storm two days before the first pass. On the first pass the field strength was depressed from 4 to 8 radii by a roughly constant amount, ~25-50%, while farther out the field strength remained at ~50-75% right out to apogee at 16 radii. On the second pass there was no depression and the field strength settled at 30-50% from 10 radii out to apogee. On both passes the direction swung round and settled pointing away from the earth, the swing occurring between 7 and 9 radii on the first pass and between 9 and 11 radii on the second pass. It is this change in direction observed on Explorer 10, both published passes of Explorer 14 and unpublished passes of Explorer 14 (Cahill, private communication) which resembles the change in field direction observed by Explorer 6 near apogee. The far field

near the noon meridian was observed by Explorer 12 [Cahill and Amazeen, 1963] and behaves entirely differently, demonstrating that the distortion is quite asymmetric and therefore not due to a ring current alone.

The observations seem to fit Dungey's model, though further measurements are required to fill in the picture. The outstanding features in this theoretical model are two concentrated current sheets, in both of which the current flows in the direction opposite to the orbital motion of the earth, the return current not being concentrated in sheets. One sheet is on the day side, is oriented normal to the direction of the sun, contains current flowing eastward, and has been found by Explorer 12. The other is on the night side, oriented roughly in the equatorial plane, contains current flowing westward, and has not yet been found. The existence of the latter current sheet is, however, consistent with the observations far out and south of the equatorial plane. Because the sheet current is westward, the effect at 6 radii is hard to distinguish from the effect of a ring current, and the nature of the distinction needs consideration.

#### Distinction Between the Ring Current and Distortion by the Solar Wind

It has been stated that the ring current can be derived from the balance between the anisotropic pressure of the trapped particles and the force density  $j \times B/c$ . The distortion by the wind is derived by consideration of the plasma flow resulting from the imbalance between these same forces, but only a qualitative theoretical picture has yet been obtained. However, this shows that the two effects cannot be distinguished rigorously in terms of physical mechanisms, and this is true a fortiori if the trapped particles originate from the solar wind

as seems likely because of their storm time variation. The distinction can then only be geometrical. The axial symmetry of the ring current contrasts with the asymmetry of the observed field far out, and it is clear that the relative importance of the wind distortion increases with the distance from the earth. Both disturbances are established beyond reasonable doubt, but it will never be easy to make a rigorous separation of the two.

#### ACKNOWLEDGMENTS

This work was supported financially by the National Aeronautics and Space Administration under contract NASw-270. We are grateful to Space Technology Laboratories, Inc., and particularly to Dr. Rosen and the Space Physics Department for their cooperation and assistance in the performance of this task. Technical assistance was provided by J. Kinsey, N. Lyke, and G. Komatsu of the Space Physics Department and by I. Kliger and P. Lipinski of the Computation and Data Reduction Center.

We want to express our appreciation also to our colleagues, P. J. Coleman, Jr., who was involved in the initial effort to reduce the phase data, K. Moe for his careful refinement of the Explorer 6 trajectory, Prof. J. A. Simpson and Prof. J. Winckler for making ground station and satellite data available to us, and Dr. A. J. Dessler and Dr. R. C. Wentworth for many helpful discussions regarding ring current theory.



REFERENCES

- Akasofu, S. I., Deformation of magnetic shells during magnetic storms, J. Geophys. Res., 68, 4437-4445, 1963.
- Akasofu, S. I., J. Cain, and S. Chapman, The magnetic field of a model radiation belt, numerically computed, J. Geophys. Res., 66, 4013, 1961.
- Akasofu, S. I., and S. Chapman, The ring current, geomagnetic disturbance and the Van Allen belts, J. Geophys. Res., 66, 1321, 1961.
- Apel, J. R., S. F. Singer, and R. C. Wentworth, Effects of trapped particles on the geomagnetic field, Advances in Geophysics, g, edited by H. E. Landsberg and J. V. Miegum, Academic Press, New York, 1962, 131.
- Arnoldy, R. L., R. A. Hoffman, and J. R. Winckler, Observations of the Van Allen radiation during August and September 1959, Part I. J. Geophys. Res., 65, 1361, 1960.
- Cahill, L. J., Jr., Preliminary results of magnetic field measurements in the tail of the geomagnetic cavity, in press, 1963.
- Cahill, L. J., and P. G. Amazeen, The boundary of the geomagnetic field, J. Geophys. Res., 68, 1835-1843, 1963.
- Coleman, P. J., C. P. Sonett, D. L. Judge, and E. J. Smith, Some preliminary results of the Pioneer 5 magnetometer experiment, J. Geophys. Res., 65, 1856, 1960.
- Davis, L. R., and J. M. Williamson, Low energy trapped protons, in Space Research, Proc. Intern. Space Sci. Symp., 3rd, Washington, 1962, North-Holland Publishing Company, Amsterdam, 1963.
- Dungey, J. E., Null point in space plasmas, Symp. on Plasma Space Sci., The Catholic University of America, June 11-14, 1963.
- Fan, E. Y., P. Meyer, and J. A. Simpson, Trapped and cosmic radiation measurements from Explorer 6, in Space Research, edited by H. Kallman-Bijl, p. 951, North-Holland Publishing Company, Amsterdam, 1960.

- Heppner, J. P., N. F. Ness, C. S. Scearce, and T. L. Skillman, Explorer 10 magnetic field measurements, J. Geophys. Res., 68, 1-46, 1963.
- Heppner, J. P., J. D. Stolarik, I. R. Shapiro, and J. C. Cain, Project Vanguard magnetic field instrumentation and measurements, in Space Research, Proc. Intern. Space Sci. Symp., 1st, 1960, edited by H. Kallman-Bijl, p. 982, North-Holland Publishing Company, Amsterdam, 1960.
- Judge, D. L., A. R. Sims, and M. G. McLeod, The Pioneer 1, Explorer 6, and Pioneer 5 high sensitivity transistorized search coil magnetometer, I. R. E. Trans. on Space Elect. and Telem., SET 6, 114, 1960.
- Krassovsky, V. I., Results of scientific investigations made by Soviet sputniks and cosmic rockets, Astronaut. Acta, 6, 32, 1960.
- Lincoln, J. V., Geomagnetic and solar data, J. Geophys. Res., 65, 788, 1960.
- Midgley, J. E., and L. Davis, Jr., Calculation by a moment technique of the perturbation of the geomagnetic field by the solar wind, J. Geophys. Res., 68, 5111-5123, 1963.
- Neugebauer, M., and C. W. Snyder, The solar plasma experiment (in Mariner 2), Science, 138, 1095-1097, 1962.
- Rosen, A., and T. A. Farley, Characteristics of the Van Allen radiation zones as measured by the scintillation counter on Explorer 6, J. Geophys. Res., 66, 2013-2028, 1961.
- Smith, E. J., P. J. Coleman, D. L. Judge, and C. P. Sonett, Characteristics of the extraterrestrial current system: Explorer 6 and Pioneer 5, J. Geophys. Res., 65, 1858, 1960.
- Smith, E. J., and D. L. Judge, Transient variations in the extraterrestrial magnetic field (abstract), J. Geophys. Res., 66, 2562, 1961.

- Smith, E. J., and C. P. Sonett, Satellite observations of the distant field during magnetic storms: Explorer 6, Proc. Intern. Conf. on Cosmic Rays and the Earth Storm, Kyoto, Sept. 1961, J. Phys. Soc., Japan 17, 17, 1962.
- Smith, E. J., A comparison of Explorer 6 and Explorer 10 magnetometer data, J. Geophys. Res., 67, 2095, 1962.
- Sonett, C. P., D. L. Judge, and J. M. Kelso, Evidence concerning instabilities in the distant geomagnetic field: Pioneer 1, J. Geophys. Res., 64, 941, 1959.
- Sonett, C. P., D. L. Judge, A. R. Sims, and J. M. Kelso, A radial rocket survey of the distant geomagnetic field, J. Geophys. Res., 65, 55, 1960.
- Sonett, C. P., E. J. Smith, and A. R. Sims, Surveys of the distant geomagnetic field: Pioneer 1 and Explorer 6, in Space Research, Proc. Intern. Space Sci. Symp., 1st, 1960, edited by H. Kallman-Bijl, p. 921, North-Holland Publishing Company, Amsterdam, 1960.
- Sonett, C. P., E. J. Smith, D. L. Judge, and P. J. Coleman, Current systems in the vestigial geomagnetic field: Explorer 6, Phys. Rev. Letters, 4, 161, 1960.
- Vestine, E. H., Lines of force of the geomagnetic field in space, Planet. and Space Sci., 1, 285, 1959.

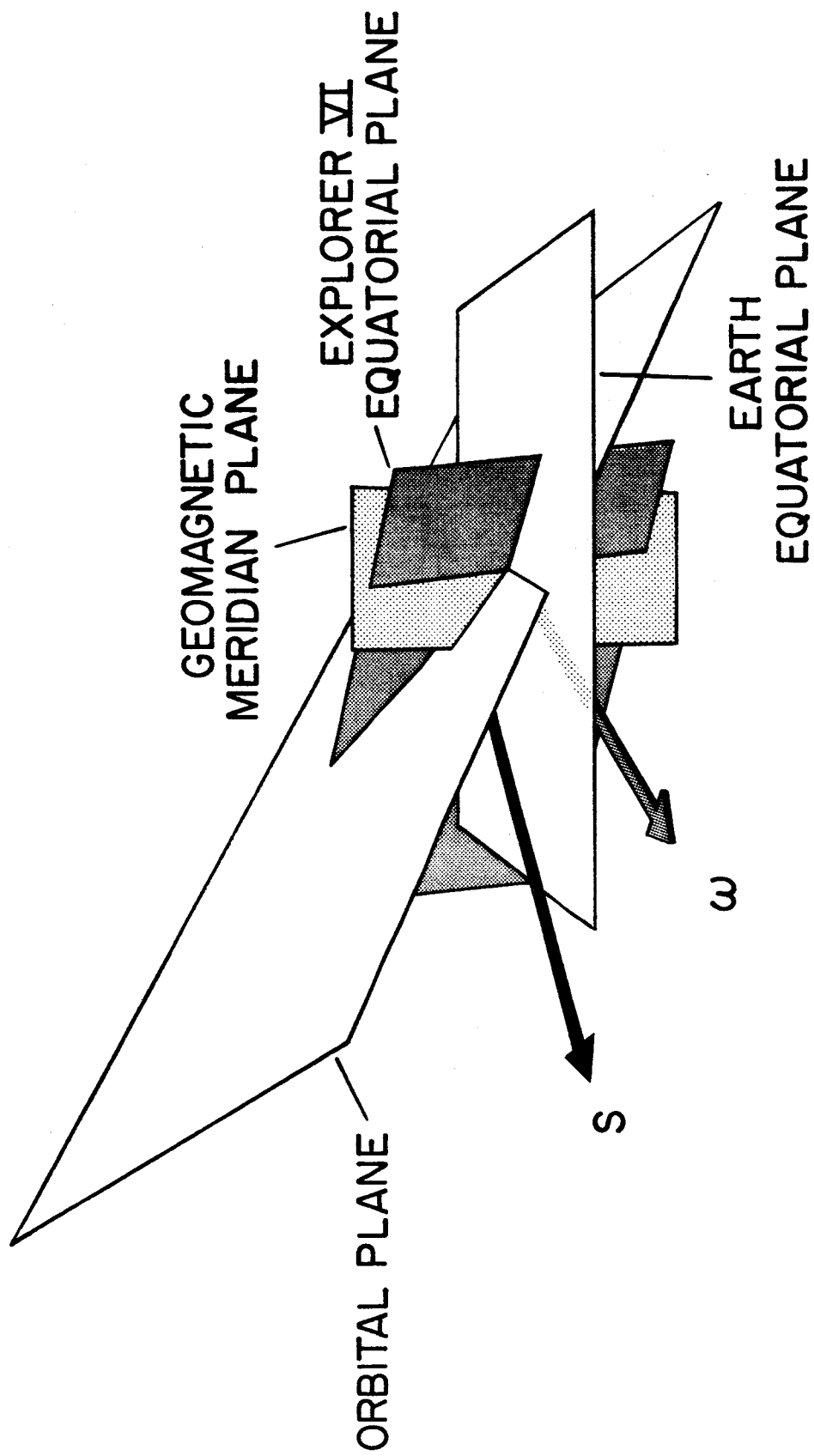


Figure 1.- Explorer 6 orbital geometry.

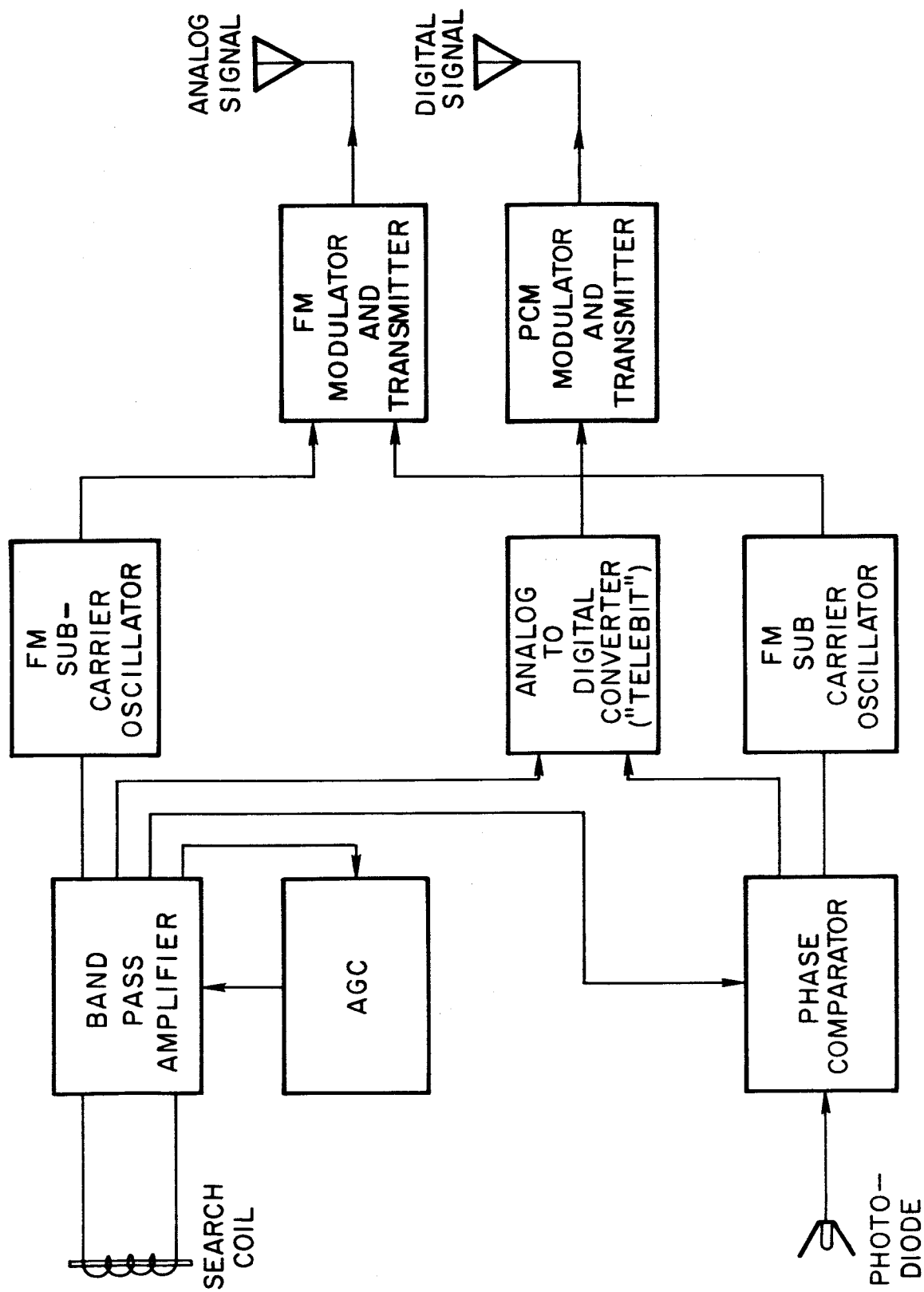


Figure 2.- Block diagram of the search coil magnetometer.

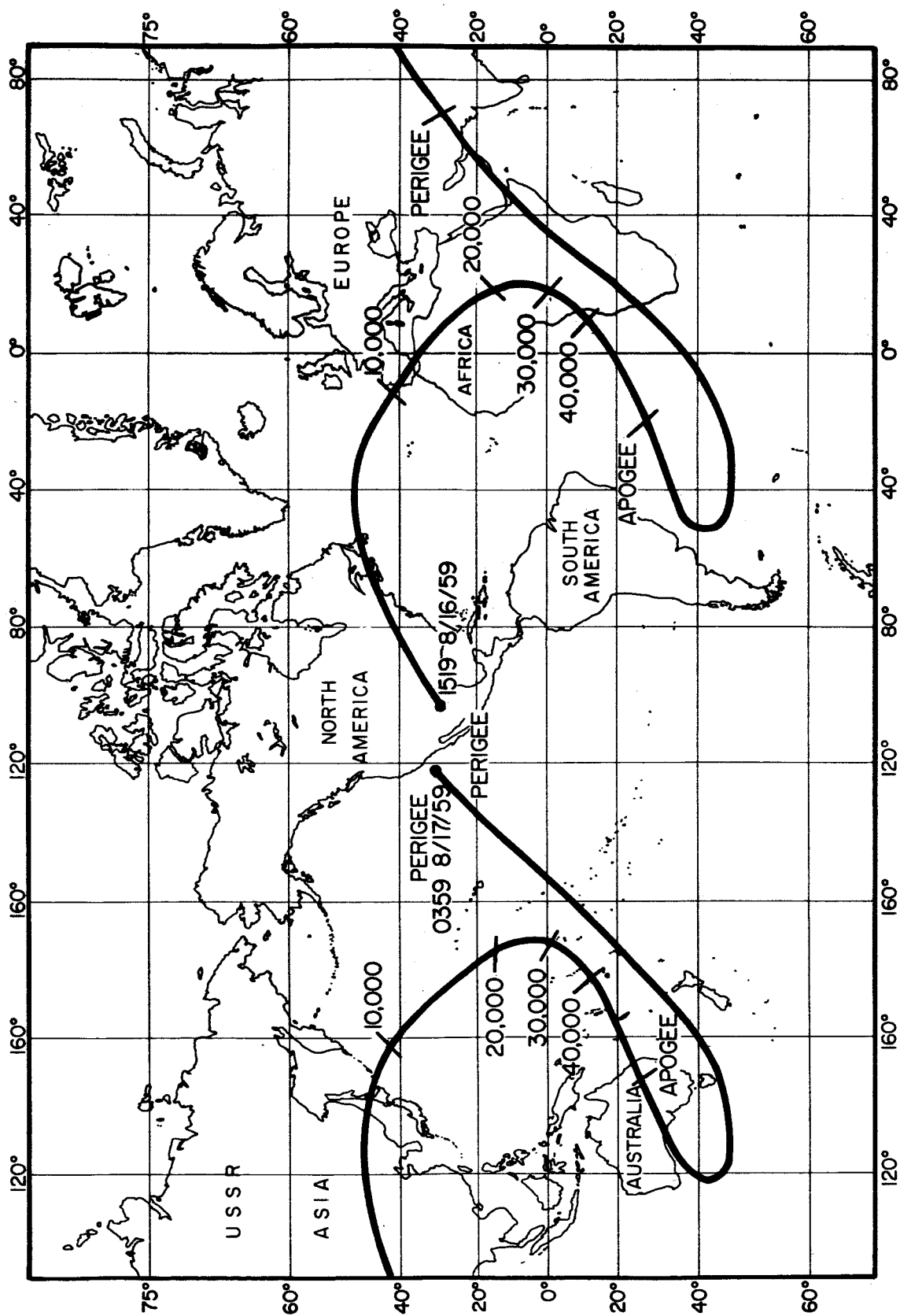


Figure 3.- Projection of the Explorer 6 trajectory onto the earth.

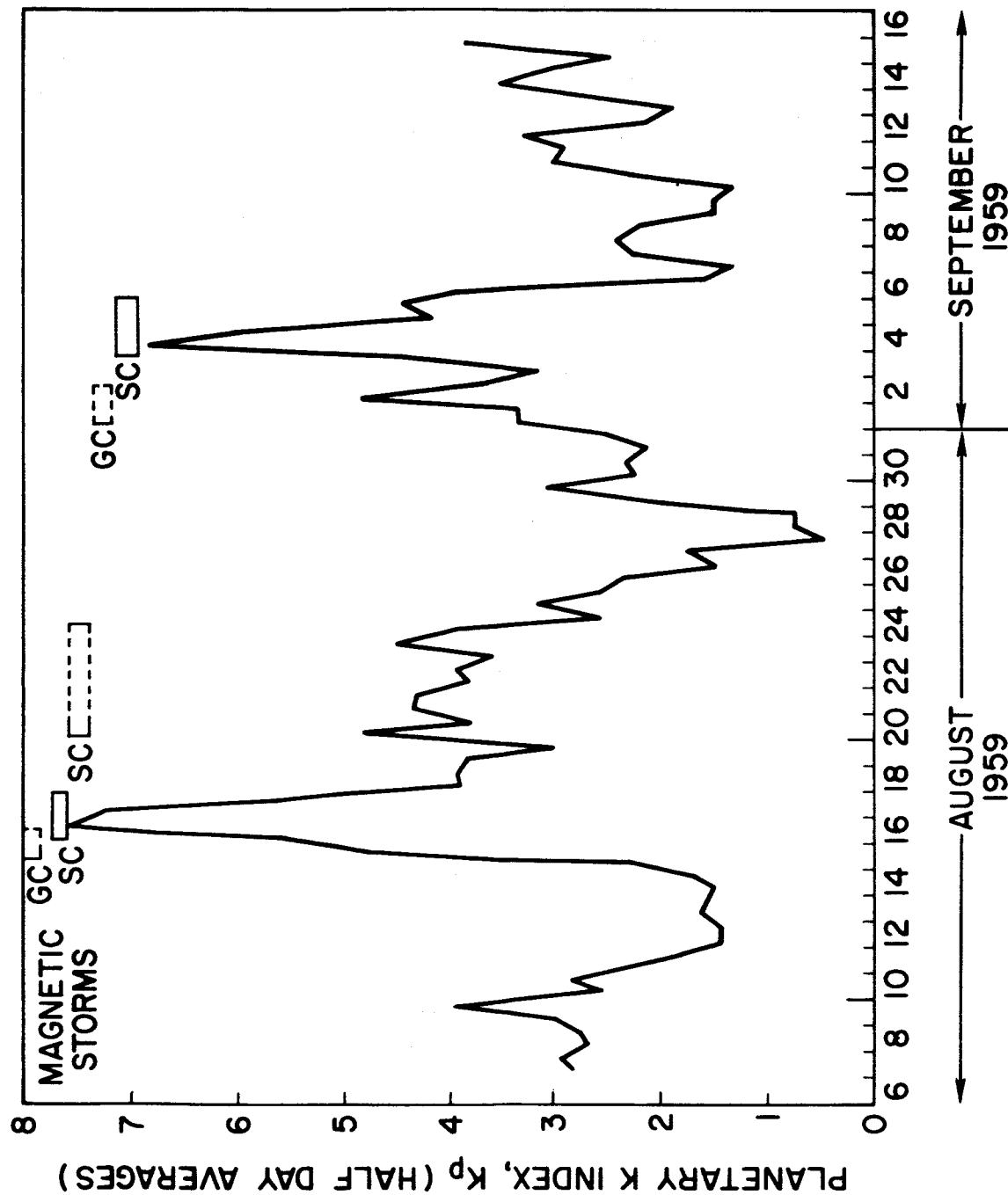


Figure 4.- Geomagnetic activity during the Explorer 6 epoch.

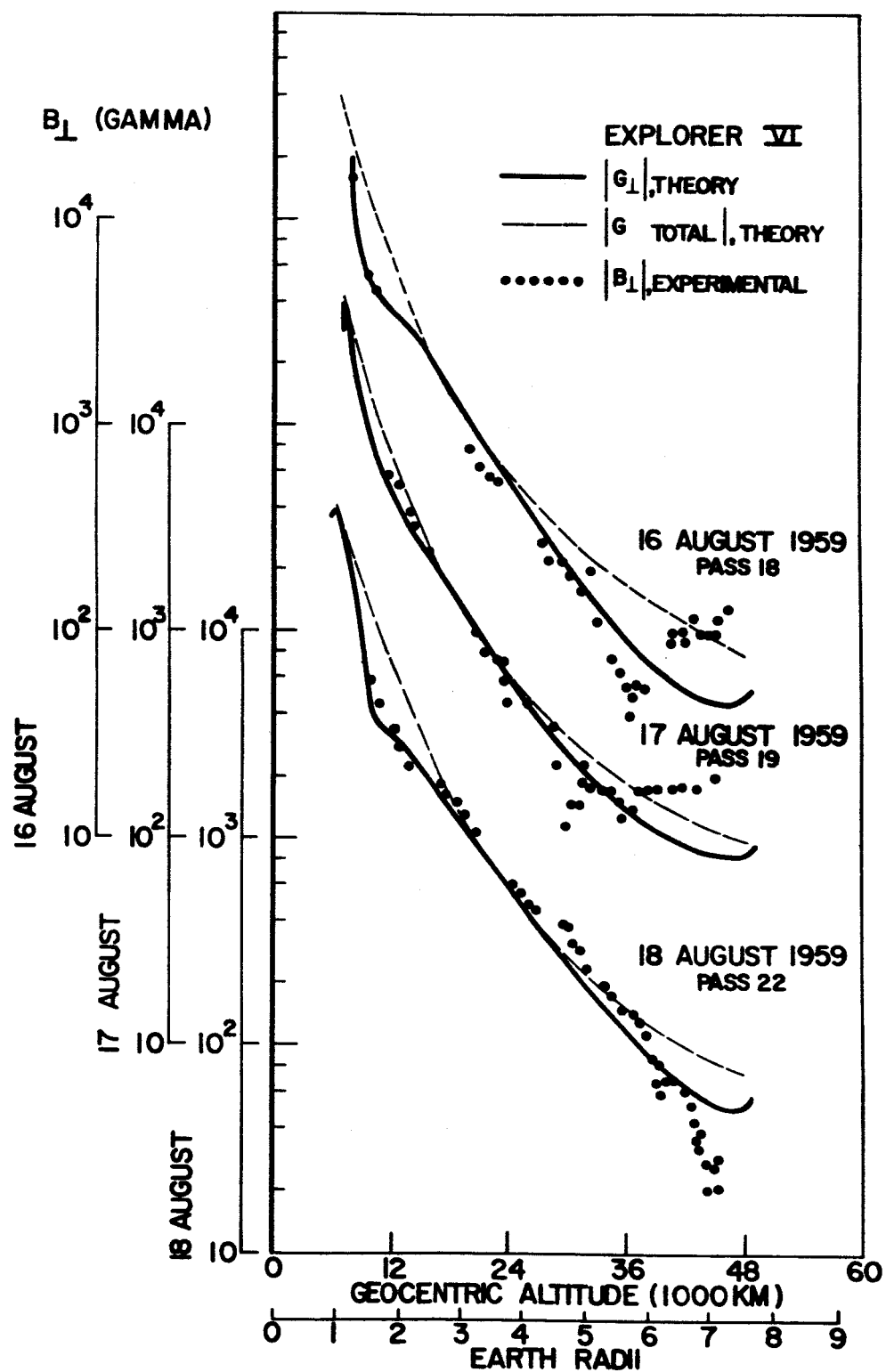


Figure 5.- Explorer 6 field magnitude data during the magnetic storm of 16-18 August, 1959.



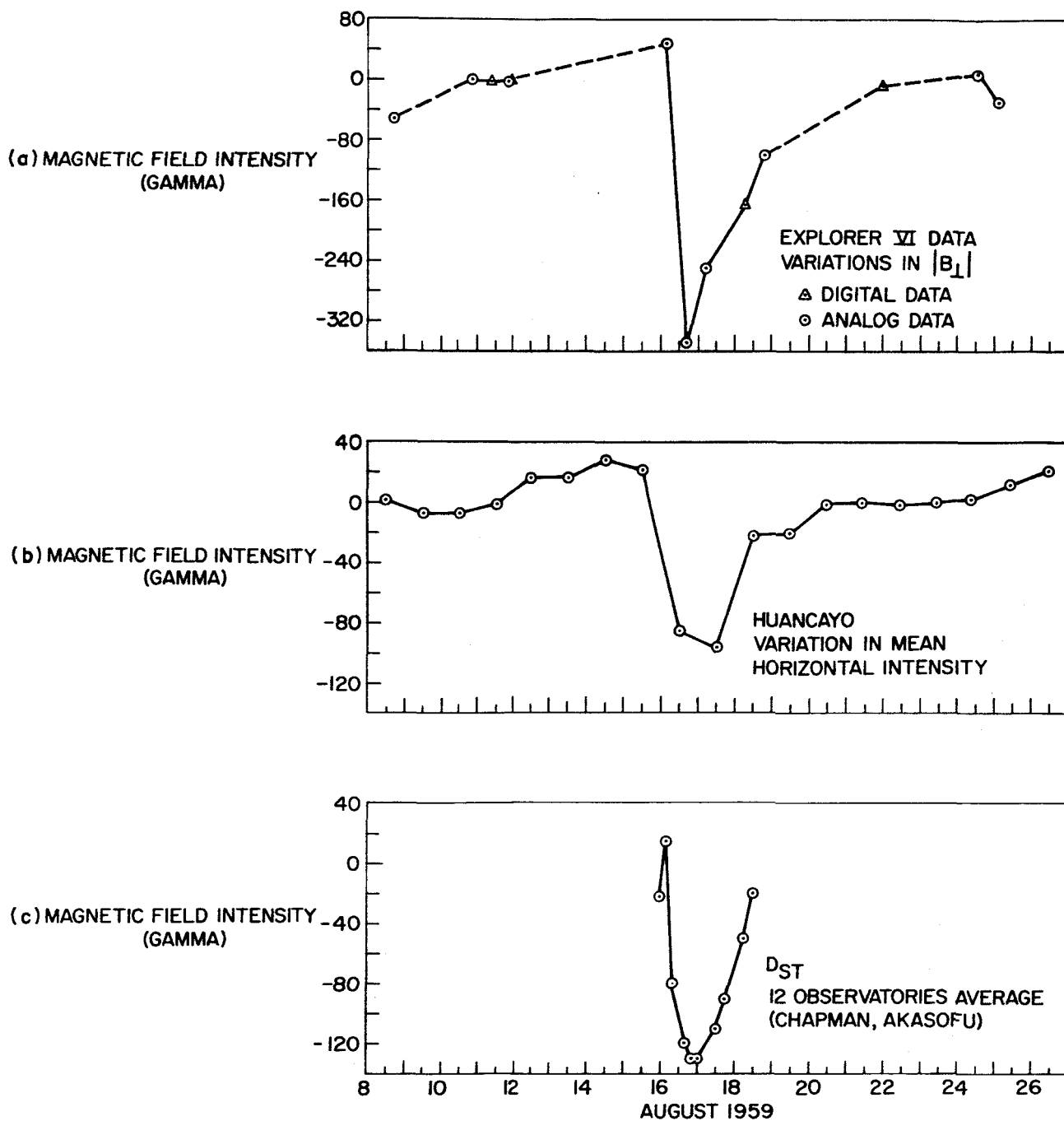


Figure 6.- Time variations of the equatorial disturbance field compared with  $D_{ST}$  variations at the earth's surface.

# EXPLORER VI MAGNETOMETER PHASE ANGLE

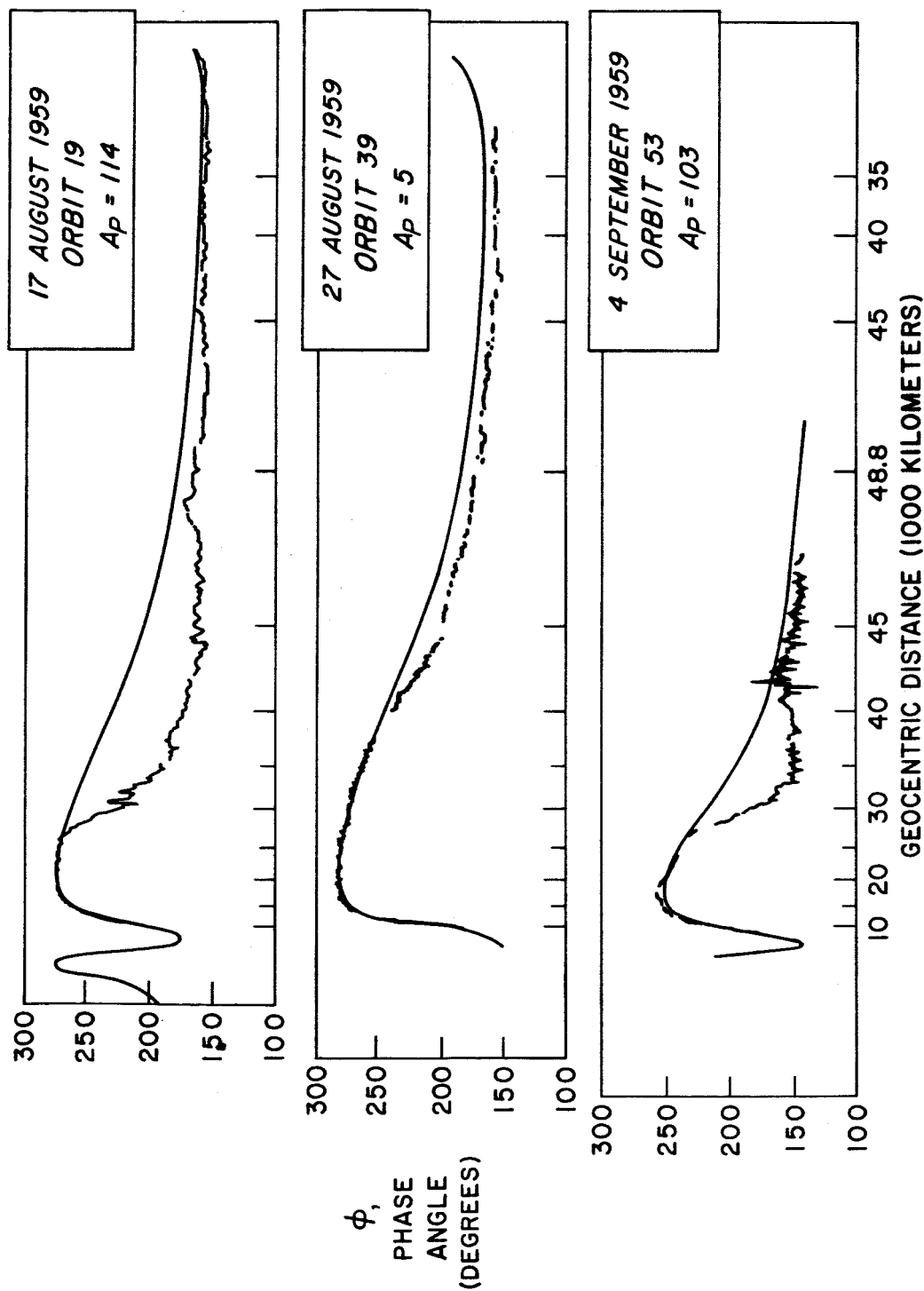


Figure 7.- Phase angle data during storm and nonstorm intervals.

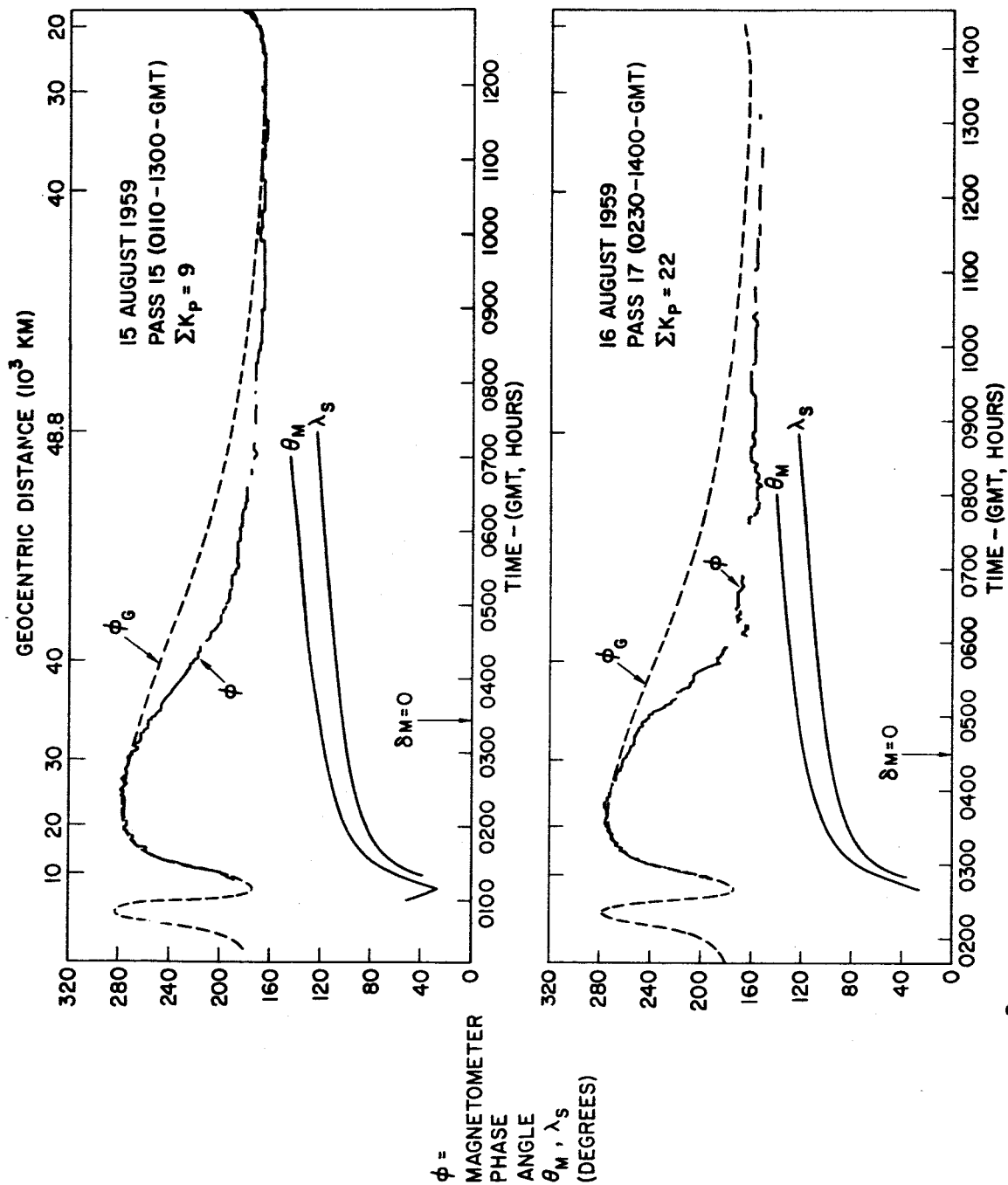
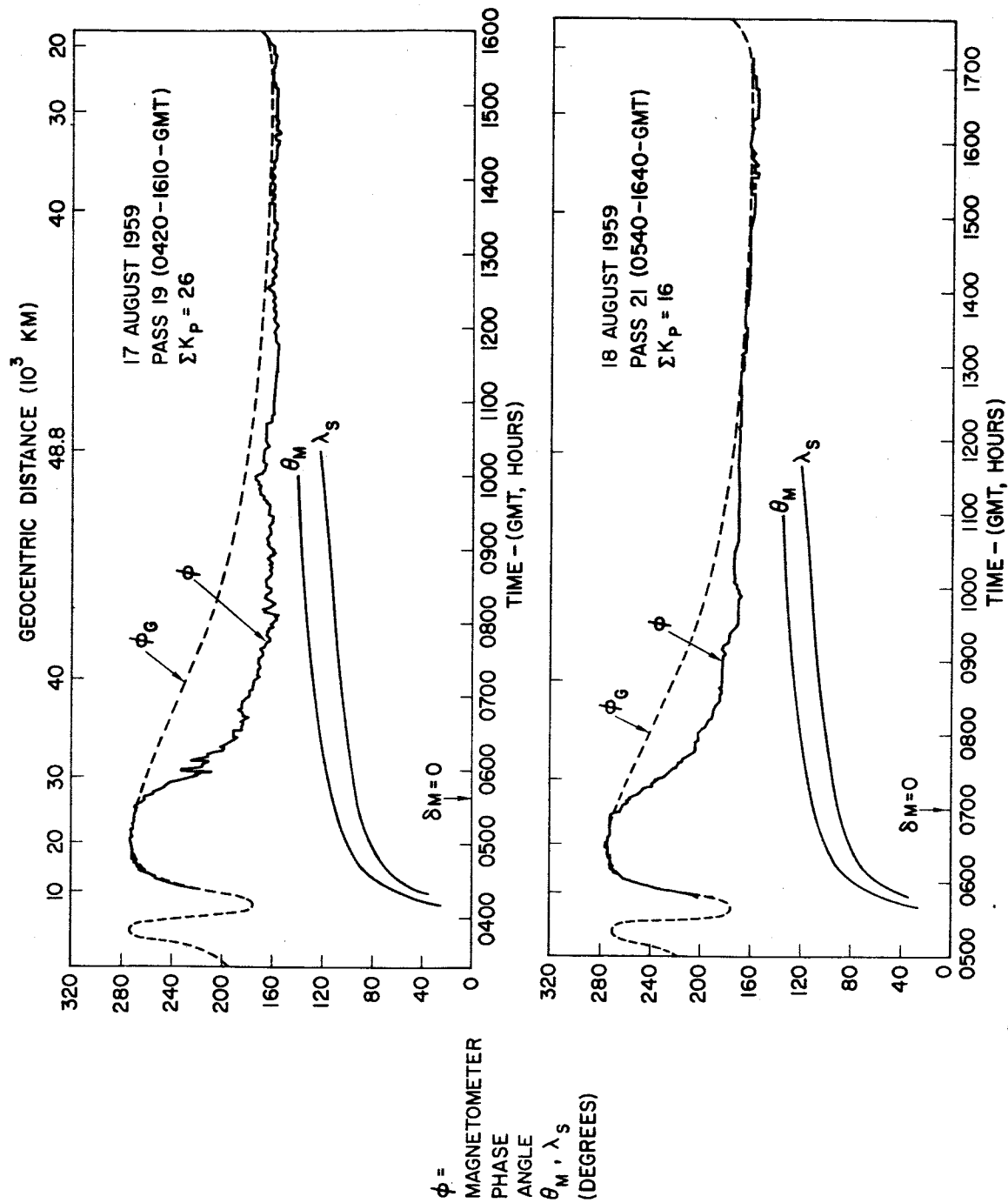
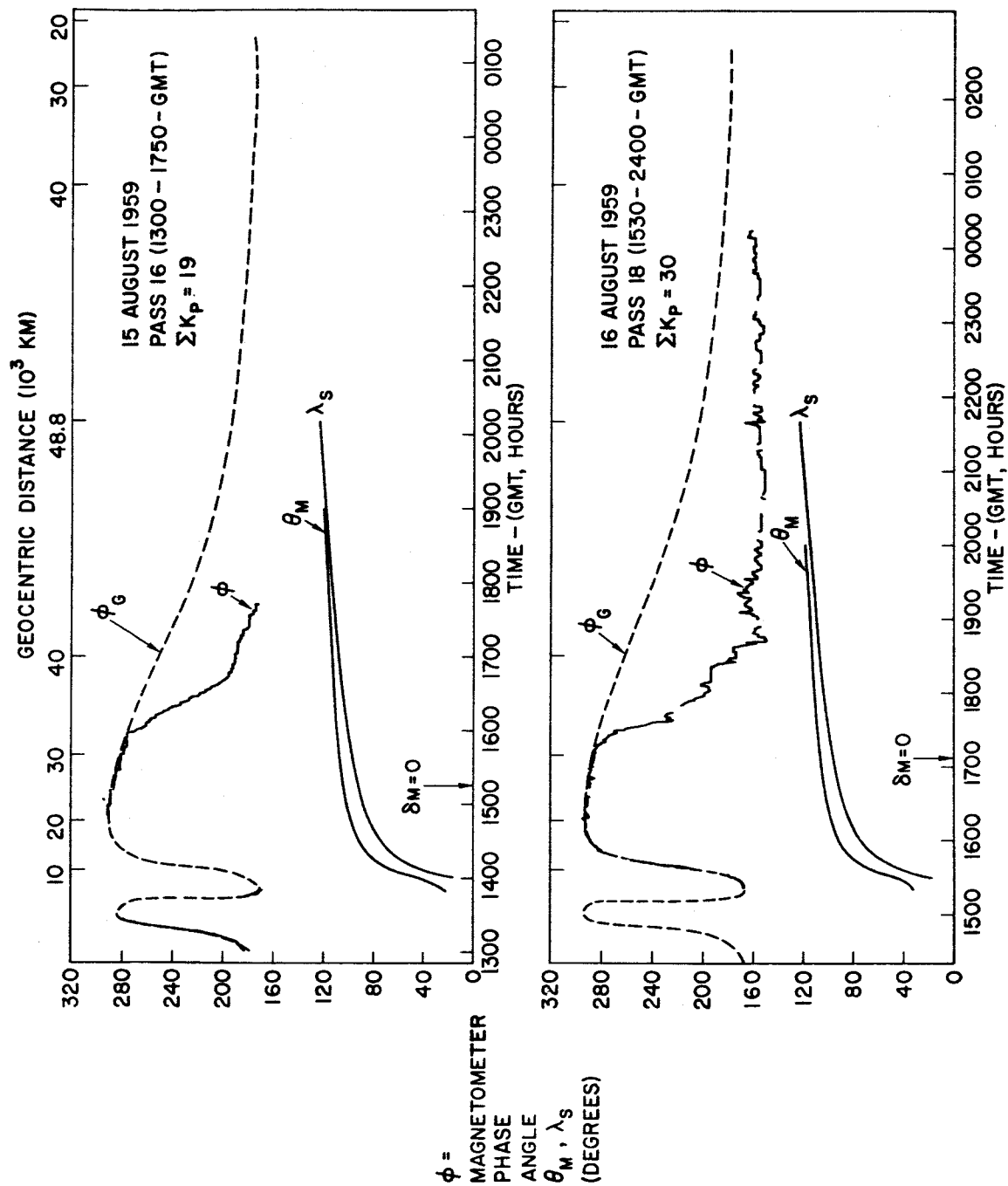


Figure 8.- Phase data obtained during a magnetic storm (odd numbered passes).



9  
 Figure 16.- Phase data obtained during a magnetic storm (odd numbered passes).



10  
 Figure 11.- Phase data obtained during a magnetic storm (even numbered passes).

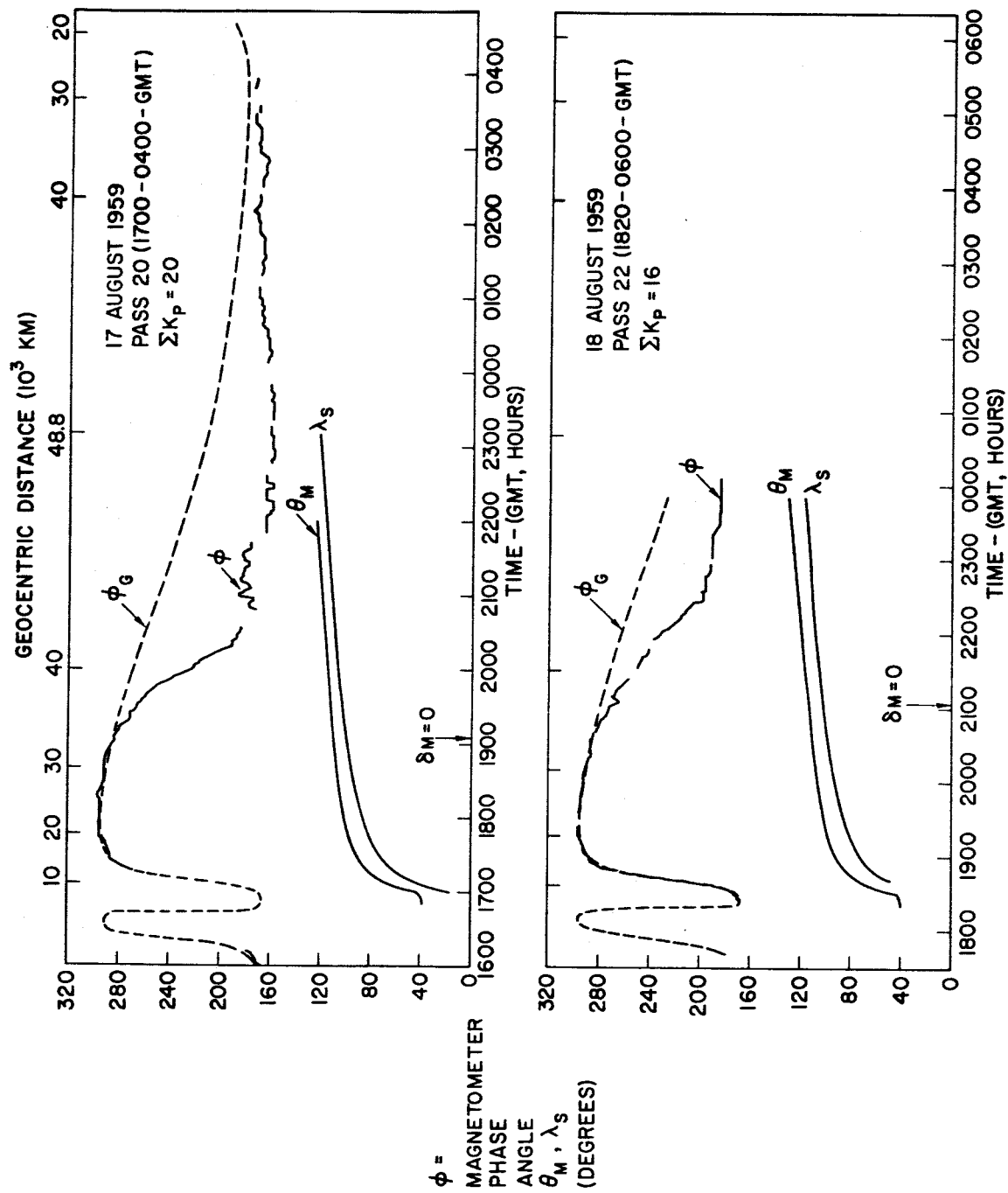
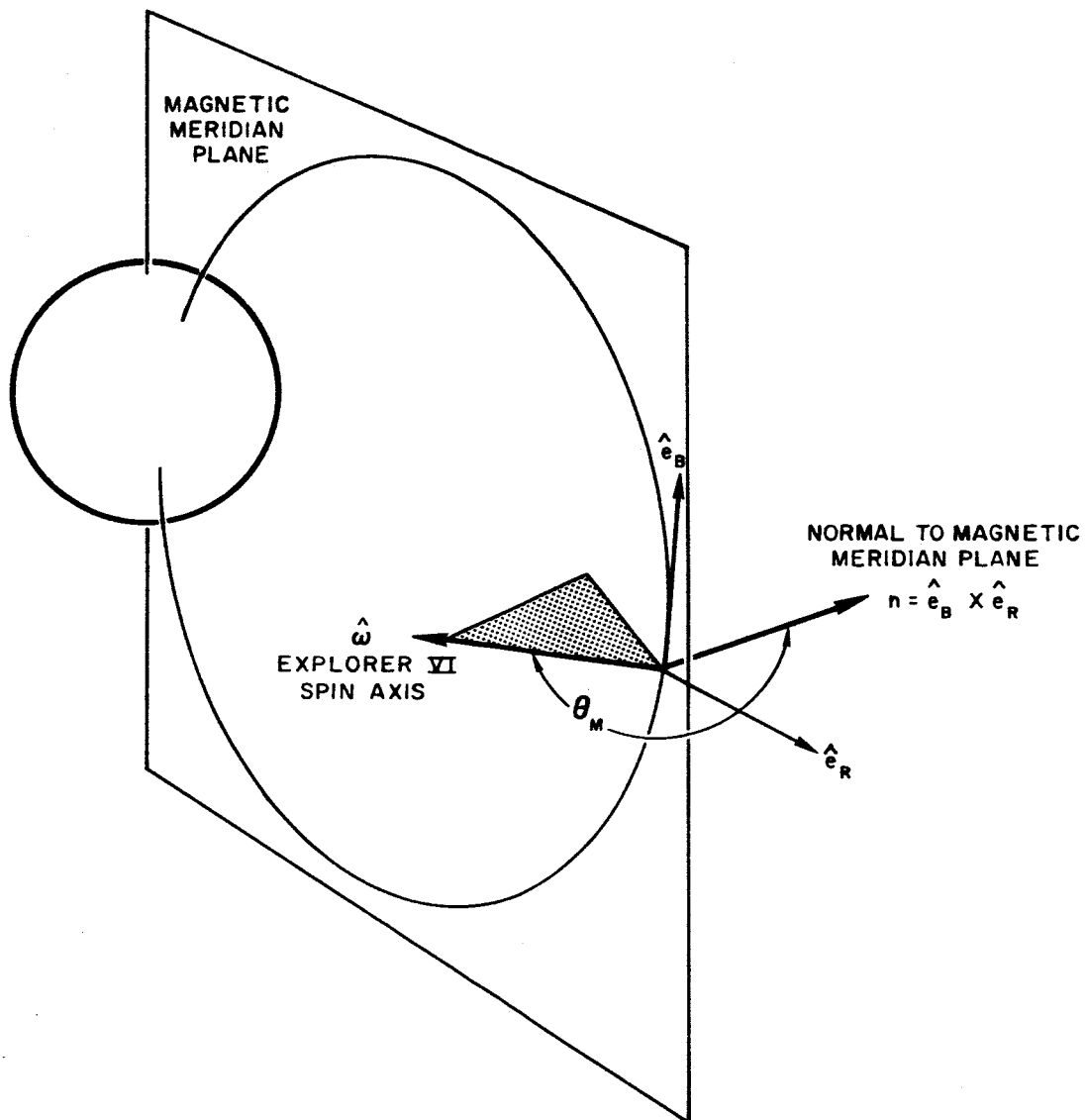
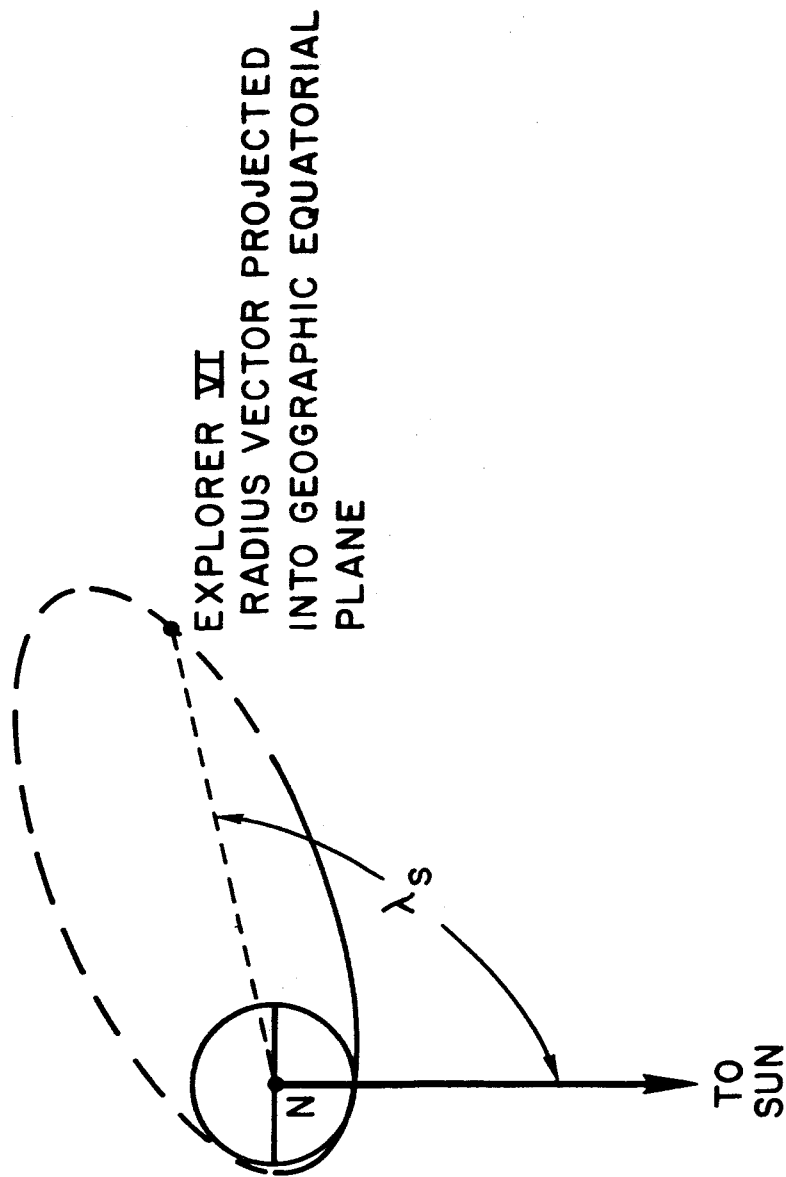


Figure 11. - Phase data obtained during a magnetic storm (even numbered passes).



$\hat{e}_B$ , UNIT VECTOR IN DIRECTION OF GEOMAGNETIC FIELD  
 $\hat{e}_R$ , UNIT VECTOR IN DIRECTION FROM EARTH'S CENTER

Figure 12.- Representation of the angle,  $\theta_M$ .



13  
Figure 14.- Representation of the angle,  $\lambda_s$ .



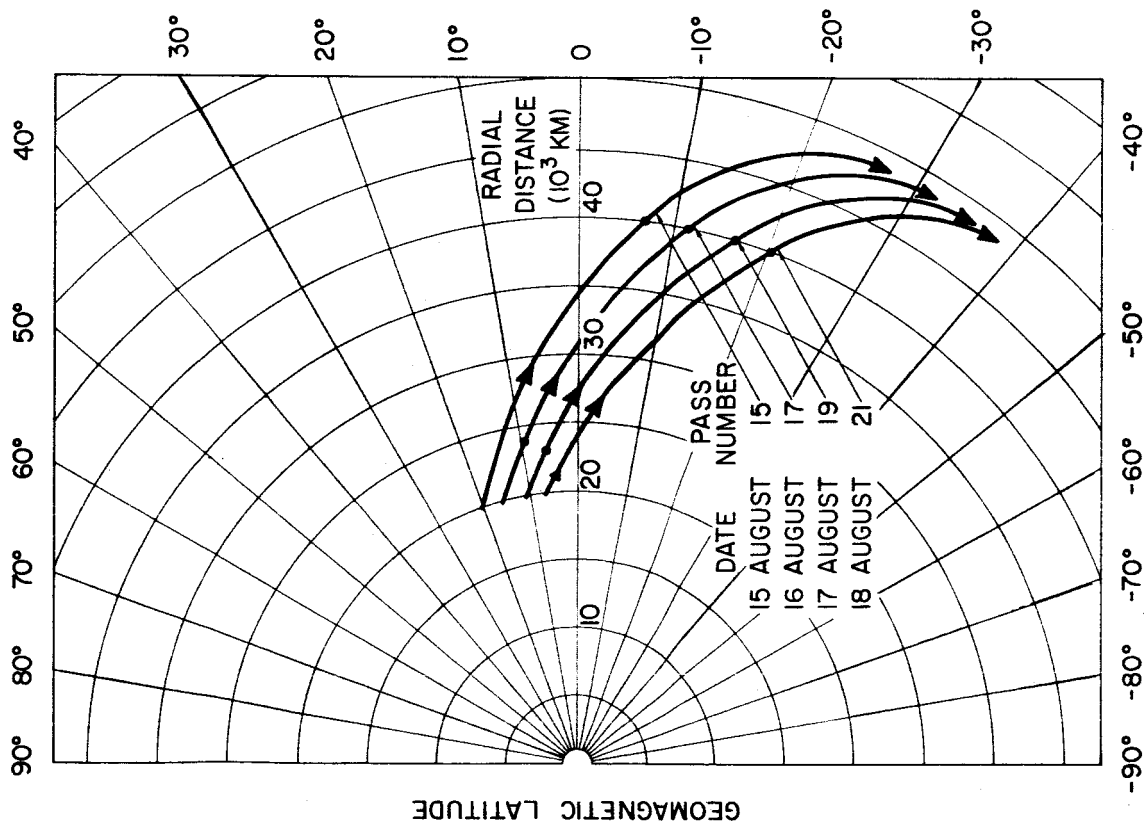


Figure 15.- Geomagnetic latitude of the spacecraft (odd numbered passes).

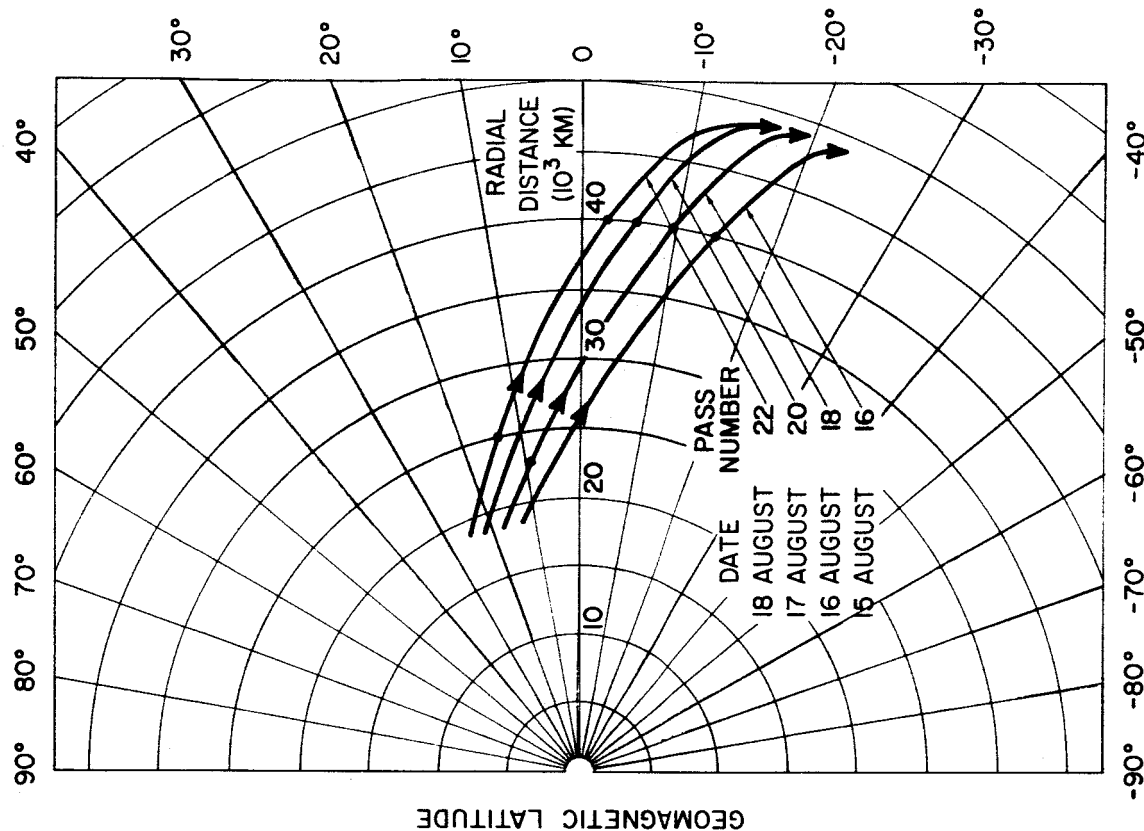
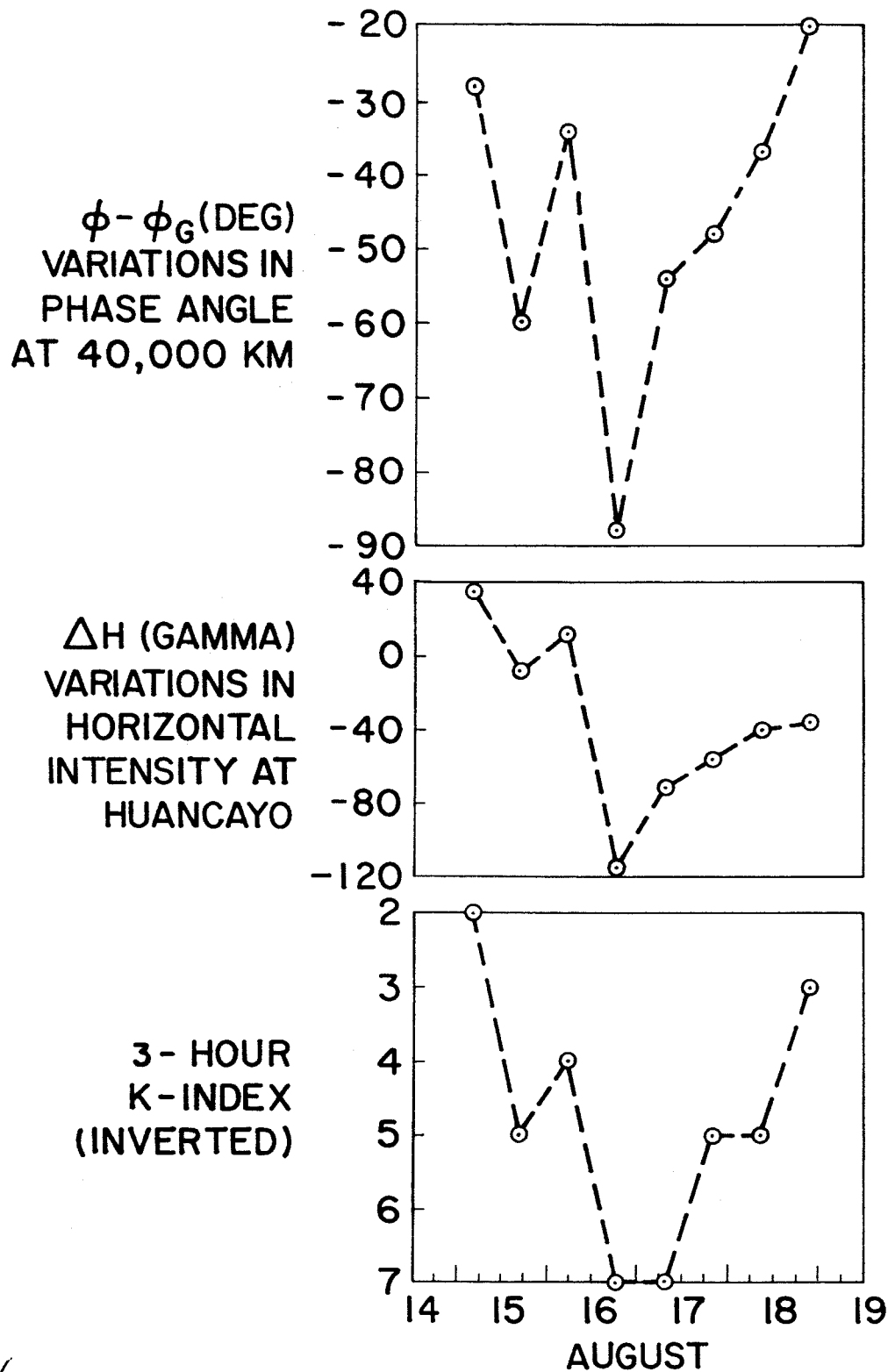


Figure 16.- Geomagnetic latitude of the spacecraft (even numbered passes).



16  
Figure 17.- Temporal variation in the phase data at 40,000 kilometers compared with the surface field.

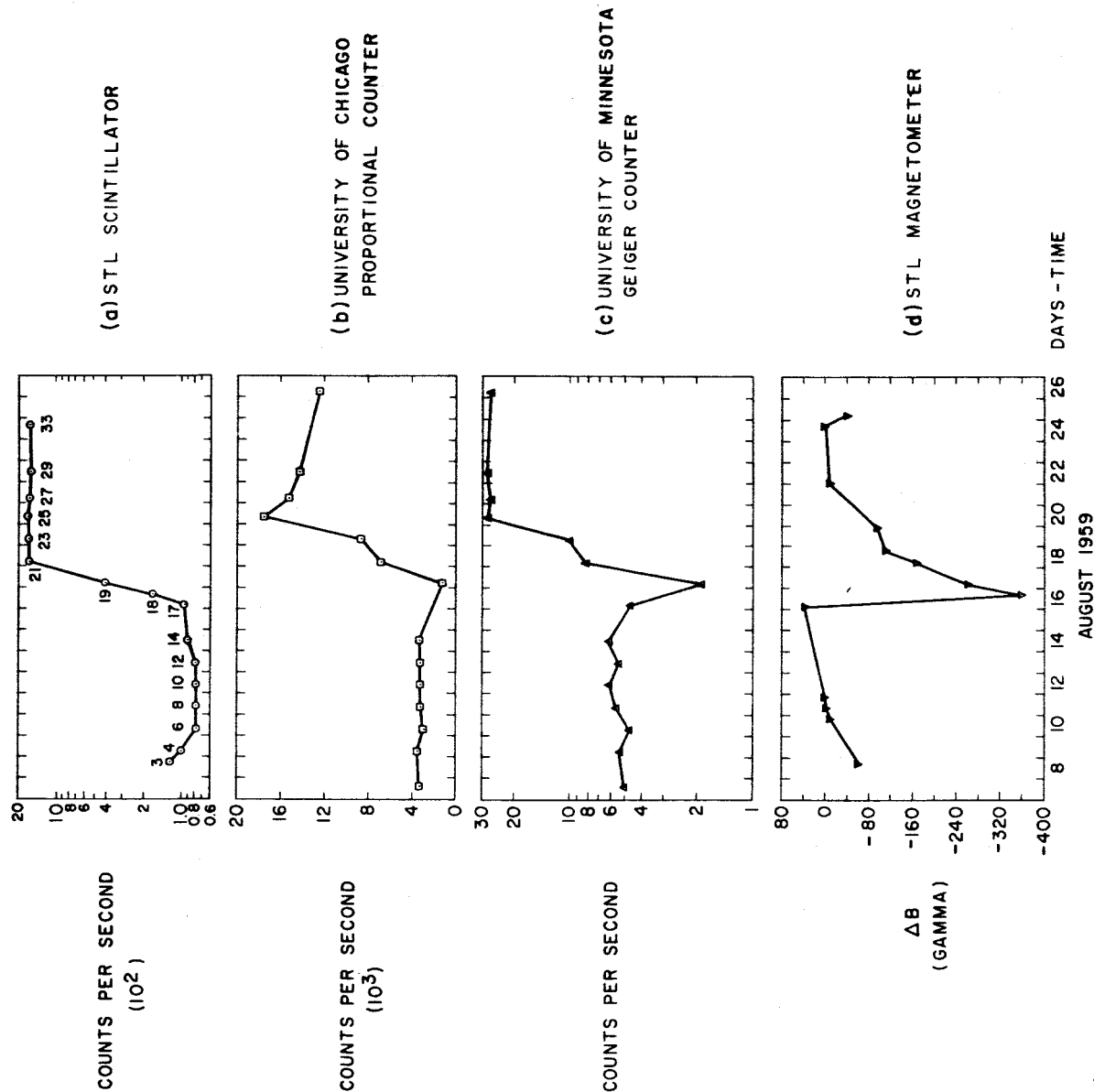


Figure 26. - Comparison of equatorial magnetic field variations at  $40^\circ E$  with simultaneous variation in the three Explorer 6 high energy particle detectors.